Journal Pre-proof

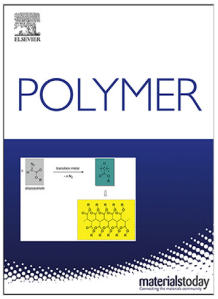

Effects of zinc oxide filler on the curing and mechanical response of alkyd coatings

Lauren F. Sturdy, Madeleine S. Wright, Alexander Yee,
Francesca Casadio, Katherine T. Faber, Kenneth R. Shull

PII: S0032-3861(20)30064-1
DOI: https://doi.org/10.1016/j.polymer.2020.122222
Reference: JPOL 122222

To appear in: *Polymer*

Received date : 5 December 2016
Revised date : 5 January 2020
Accepted date : 22 January 2020

Please cite this article as: L.F. Sturdy, M.S. Wright, A. Yee et al., Effects of zinc oxide filler on the curing and mechanical response of alkyd coatings, *Polymer* (2020), doi: https://doi.org/10.1016/j.polymer.2020.122222.

Effects of Zinc Oxide Filler on the Curing and Mechanical Response of Alkyd Coatings

Lauren F. Sturdy[1], Madeleine S. Wright[1], Alexander Yee[1], Francesca Casadio[2], Katherine T. Faber[3] and Kenneth R. Shull[1]

[1]*Department of Materials Science and Engineering, Northwestern University, USA*
[2]*The Art Institute of Chicago, USA*
[3]*Division of Engineering and Applied Science, California Institute of Technology, USA*

Abstract

The mechanical properties of an alkyd resin filled with zinc oxide pigment were studied at different concentrations over a wide range of time scales using dynamic mechanical analysis, quartz crystal rheometry and nanoindentation. The motivation for this work stems from the interest in accessing the long-term properties of paint coatings by studying the mechanical properties of historic paints. In this foundational work, we compare three different modalities of mechanical measurements and systematically determine the effect of pigment filler loading on the measured properties. Quantitative agreement between the methods is obtained when the characteristic time scales of each of the methods is taken into account. While nanoindentation is the technique most readily applied to historic paint samples, the rheometric quartz crystal microbalance (rheo-QCM) is the best suited for obtaining mechanistic information from measurements of paint properties over time, provided that appropriate thin-film samples can be produced. In these studies we find that ZnO increases the rate of oxidation of the alkyd during the initial stages of cure by an amount that depends on the ZnO content.

1. Introduction

The pigments which give paints their distinctive colors are of obvious importance to the overall paint formulation. These pigments can be organic or inorganic, and since each pigment has its own chemical makeup, pigments interact chemically with paint binders in different ways [1, 2]. The chemistry, particle shape/size and amount of pigment present in a paint will also affect the overall paint properties and performance such as covering power, viscosity, and curing time. Previous studies have demonstrated that properties of polymeric binder/pigment systems are dependent on the pigment volume contained within the binder [3–5]. The inclusion of rigid pigment particles in a flexible binder constrains its mobility, just as the stiff cross-links in the resin itself do [6]. A critical pigment volume fraction can generally be identified for a given system, representing the most densely packed distribution of pigment particles that can be obtained without the introduction of voids [3, 6]. The stiffness of paint films increases with increasing pigment concentration, with very strong effects observed near the critical concentration. This effect has been investigated quite extensively in a variety of related materials systems, ranging from ceramic slurries to polymer

emulsions. In situations where the particles are much stiffer than the continuous matrix phase, the modulus increases with filler volume fraction. While a variety of functional forms have been used to quantify this behavior in different systems [7–12], the following expression for the shear modulus, G, similar to the form suggested by Krieger and Doherty for suspensions of monodisperse spheres,[7] is representative:

$$G = G_0 \left(1 - \phi/\phi^*\right)^{-2} \tag{1}$$

Here G_0 is the shear modulus of the unfilled matrix material and ϕ^* plays the role of a the critical pigment concentration in a paint formulation. For a viscoelastic material a similar expression can be used, with G replaced by the complex dynamic shear modulus, G^*, which is now a function of the frequency at which the measurement is performed. For viscoelastic materials the functional form of the concentration dependence may be a function of the frequency, as is indeed the case for the model paint systems investigated in this work.

Much of the complexity of pigmented systems originates from the fact that the pigment affects the properties of the binding medium, so that G_0 is now also a function of ϕ. Systematic investigations with model systems are therefore needed in order to decouple these effects, and to understand the role that pigment particles have on modifying the intrinsic properties of the binder. These effects are known to be quite important, including, for example the well-documented role of ZnO pigments on the degradation of oil-based paints resulting from the formation of metal soaps. [13–18].

The aim of the work reported here is to investigate pigment-induced changes in the mechanical properties of an alkyd binder by directly studying the mechanical response of a series of samples filled with zinc oxide. Zinc oxide is a particularly relevant filler material that has been used as a white pigment in artists' paints since the late 18th century [14, 19]. In natural aging studies of linseed oil pigmented with a variety of organic and inorganic pigments, the zinc oxide film was the stiffest and most brittle of all of the films after 12–15 years of aging [20]. Marked brittleness was also observed in alkyd resins containing zinc oxide, even in the presence of other pigments [1]. In our work we utilize three characterization methods, each of which probes the material on different length and time scales. Dynamic mechanical analysis is used to probe the response of macroscopic samples at frequencies from 0.1 Hz to 10 Hz. Nanoindentation is used to probe sample volumes with dimensions in the range of a micrometer, over time scales of $\sim$ 1sec. Finally, we use Quartz crystal rheometry, a newly developed technique that is well-suited for aging studies of polymer films, to probe films with thickness of $\sim$ 5 μm, at a frequency of 15 MHz. Results from these three techniques, which have been used individually in previous cultural heritage applications, are compared in order to illustrate their complementary nature and to illustrate the sort of quantitative information that can be obtained under appropriate conditions.

2. Materials and Methods

2.1. Materials

The alkyd films were prepared from Gamblin Artists Colors (Portland, OR) Galkyd mixed with Fischer Z50 zinc oxide ranging from 0.05 to 0.60 wet weight fraction. When necessary to change

the viscosity for stirring or film formation, Gamsol odorless mineral spirits (Gamblin Artists Colors) were mixed with the alkyd binder and zinc oxide. Samples were either ground with a mortar and pestle for ten minutes or stirred in a high speed mixer (SpeedMixer, FlackTek, Inc., Landrum, SC) for 1 minute at 2000rpm. The samples were then mixed with odorless mineral spirits to obtain an appropriate viscosity for spin coating and stirred for 48 hours before making samples. This procedure was found to produce a good dispersion of the ZnO particles as described in the supplementary information. Actual ZnO weight fractions were determined by accounting for solvent in the as-received alkyd resin, as discussed in Section 3.1.

2.2. *Thermogravimetric Analysis*

To determine the precise weight fraction, and subsequently the volume fraction of pigment distributed in the alkyd binder, each paint composition was subjected to thermogravimetric analysis using a Mettler Toledo TGA SDTA 851e (Columbus, OH). Samples with a total mass of about 5 mg were analyzed after a cure time of five months. Analysis was performed under a nitrogen atmosphere; samples were held at 30°C for 3 minutes before the temperature increased to 900°C at a ramp rate of 10°C per minute.

2.3. *Scanning Electron Microscopy*

SEM images were taken of alkyd films with a Hitachi S-3400N-II scanning electron microscope (Northridge, CA) using an accelerating voltage of 25 kV.

2.4. *Dynamic Mechanical Analysis*

Samples for dynamic mechanical analysis (DMA) were made by mixing zinc oxide with alkyd to the stated weight percents. The mixtures were ground by hand in a mortar and pestle for 10 minutes and then stirred overnight. The solutions were cast onto porous polystyrene films using a Sheen adjustable film applicator. A 0.80mm shim was used leading to a 0.42mm gap. Film thicknesses after solvent evaporation ranged from 0.11mm to 0.15mm. Films were cured under ambient conditions for two months before being removed from the polystyrene substrate and tested. Data were collected from 0.1 to 10Hz from -45 to 70°C with an initial strain of 0.02 for 2vol% (5 wt%) and 4vol% (10wt%) samples, and an initial strain of 0.05 for 9 vol% (20wt%) samples.

2.5. *Quartz Crystal Rheometry*

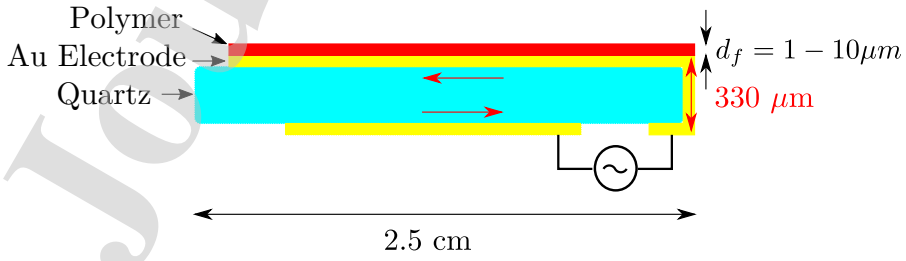

Figure 1: Schematic of the quartz crystal microbalance.

Quartz crystal rheometry is an adaptation of the use of the quartz crystal microbalance (QCM) that provides the mass per area, modulus-density product at a fixed frequency (in our case 15 MHz), and the viscoelastic phase angle at this same frequency for a film coated onto the electrode surface of a vibrating quartz crystal. The device is illustrated schematically in Figure 1. The technique is based on the fact that changes in the electrical impedance across the quartz crystal, after the film is placed on it, are proportional to the load impedance of the film as expressed in the following way [21]:

$$\frac{\Delta f_n^*}{f_1} = \frac{iZ_n^*}{\pi Z_q} \tag{2}$$

Here Δf_n^* is the complex frequency shift, given as $\Delta f_n + i\Delta\Gamma_n$, where Δf is the frequency shift and $\Delta\Gamma$ is the shift in the bandwidth of the resonance peak. The subscript n indicates the order of the harmonic, with f_1 is being the fundamental resonant frequency of the quartz crystal (5 MHz in our case). The quantity Z_q is the shear acoustic impedance of the quartz and Z_n^* is the load impedance associated with the film. In our case we measure the crystal resonance at $n = 1$ (f_1=5 MHz) , $n = 3$ (f_3 =15 MHz) and $n = 5$ (f_5 =25 MHz). For simple cases where the film is very thin or very stiff, the dissipative contribution of the impedance ($\Delta\Gamma_n$) is negligible, and the shift f_n decreases by the Sauerbrey shift, Δf_{sn}, given by the following expression: [22].

$$\Delta f_{sn} \equiv \frac{2nf_1^2}{Z_q} d\rho \tag{3}$$

Here ρ is the film density and d is its thickness, with the product of these two quantities being the mass per unit area of the film. For thicker films, the complex frequency shift deviates from the Sauerbrey prediction in a manner that depends on two parameters: ϕ_n, the viscoelastic phase angle of the film, and d/λ_n, the film thickness divided by wavelength of a shear wave within the film. The full expression for the complex resonant frequency in this case is given by the following expression [23, 24]:

$$\frac{\Delta f_n^*}{\Delta f_{sn}} = \frac{-\tan\{(2\pi d/\lambda_n)(1 - i\tan(\phi_n/2))\}}{(2\pi d/\lambda_n)(1 - i\tan(\phi_n/2))} \tag{4}$$

By measuring the frequency response at multiple harmonics and making a physically-based assumption regarding the frequency dependence of λ_n, we are able to determine ϕ_n and λ_n. The magnitude of the complex shear modulus, $|G_n^*|$ is then obtained from the following expression for the shear wavelength:

$$\lambda_n = \frac{1}{nf_1}\left(\frac{|G_n^*|}{\rho}\right)^{1/2} \frac{1}{\cos(\phi_n/2)} \tag{5}$$

In our analysis we assume the following relationship between the harmonic number, modulus, and phase angle:

$$|G_n^*| \propto n^{\phi_n/90} \tag{6}$$

This approximation is precise for a material exhibiting power law behavior, and does not add significant error to the viscoelastic parameters obtained more generally at the third harmonic (15 MHz), which is the frequency for which we report our results. This conclusion, and the detailed method used to obtain it, is described in detail by DeNolf *et al.*[25] Additional validation of the approach with rubber systems was provided more recently by Delgado *et al.*[26]

The quartz crystals used were standard AT-cut quartz crystals from Inficon (Bad Ragaz, Switzerland) with a thickness of 333μm and a diameter of 25.4mm. The electrodes were gold with a titanium adhesion layer. Measurements were taken using a CHC-100 holder from Inficon. The reference frequencies were measured individually for each crystal at the first three odd harmonics by taking measurements every 30 seconds for an hour. These were repeated two more times for each crystal after removing and replacing the crystal in the holder. Measurements of the alkyd films were taken at the first three odd harmonics ($n = 1, 3, 5$), and two different types of calculations were used in the analysis. The first calculation, used to quantify the mass changes in the early stages of cure, is referred to as a 1:3,3 calculation, and is obtained as the solution where the measured and predicted values of Δf_1,Δf_3 and $\Delta\Gamma_3$ are in agreement with one another. A similar process was used to obtain the mass and mechanical properties at longer curing times, but in this case agreement to the model was enforced for Δf_3, Δf_5 and $\Delta\Gamma_5$. These combinations were chosen because the third and fifth harmonics generally give the most reliable data, but the fifth harmonic for the prepared film thicknesses was not resolvable during the early stages of cure.

The alkyd resin and zinc oxide were mixed either by grinding by hand for 10minutes or using a FlackTek speed mixer for 1minute at 2000rpm. The resulting mixtures were thinned in mineral spirits to obtain the desired viscosity for spin coating. The amount of mineral spirits added varied with pigment concentration. The mixtures were then stirred for 48 hours. The solutions were spun cast onto the quartz crystals using a Laurell model WS-650MZ-23NPP spin coater at 3000rpm with a 200rpm/s acceleration for a total time of 120seconds. A 0% ZnO sample was prepared with a 10-minute grinding step and 48 hours of stirring to provide a reference for what curing might occur during the grinding and stirring process. The initial time in the experiments is the end of spin coating. The resultant films had thicknesses from 4–8μm as determined by quartz crystal rheometry measurements and confirmed for some samples with profilometry.

The impedance spectra were collected with either a N2PK Vector Network Analyzer or a Saunders & Associates 250B network analyzer. Coated quartz crystals were placed in a holder and measurements were taken at intervals for at least 300 days. Samples were cured under ambient conditions (usually 22–23°C and 21–25% RH). The fitting of the impedance spectra and calculations were done using in-house MATLAB programs using the method described in DeNolf *et al.*[25] based on the underlying principles described below.

2.6. Nanoindentation

Nanoindentation is a technique that involves pressing a hard indenter of known shape into a material while monitoring the load and displacement in order to measure the hardness and elastic modulus of the material. The hardness, H, of a material is given by the ratio of the load to the projected contact area of the non-recoverable impression made in the material by the indenter. In our case we obtain the hardness from the maximum load, P_{max} (illustrated in Figure 2), and from

the corresponding projected area, A, of the hardness impression.

$$H = \frac{P_{max}}{A} \tag{7}$$

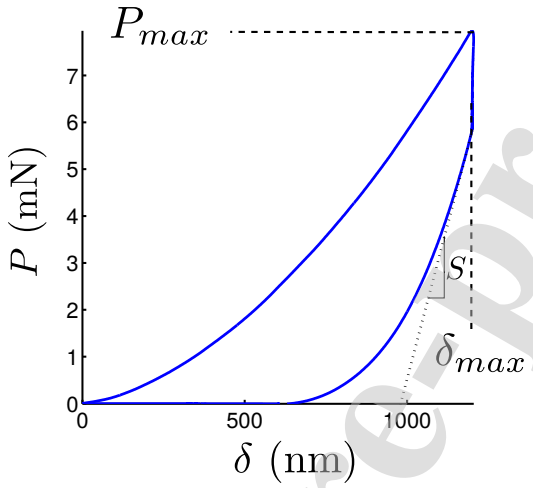

Figure 2: A typical load-displacement experiment for the indentation of the polyester resin used to embed the paint samples, labeled to illustrate the values of P_{max}, δ_{max} and S.

The projected area is related to the contact depth, δ_c, by a relationship that depends on the shape of the indenter [27]. For a Berkovich tip the appropriate relationship is:

$$A = 24.5\delta_c^2 \tag{8}$$

We follow the procedure of Oliver and Pharr and use Equation 9 to estimate the contact depth, δ_c, which is the distance between the tip of the indenter and the contact plane (see Figure 3):

$$\delta_c = \delta_{max} - 0.75\frac{P_{max}}{S} \tag{9}$$

Here δ_{max} is the maximum penetration depth of the indenter tip and S is the contact stiffness, determined experimentally as the initial slope of the linear portion of unloading curve (see Figure 2). Since the material is viscoelastic, a well-defined hold period is introduced before the unloading to allow for relaxation. The stiffness is calculated from the unloading curve after this hold period. Note that in our protocol δ is fixed at δ_{max} during the indentation, as opposed to constant-load protocol where P remains fixed at P_{max} during the relaxation phase of the experiment. The constant displacement protocol that we employ is more appropriate, since the boundary conditions of the contact problem (in this case the contact area, A) is expected to remain fixed during the indentation, resulting in a more well-defined contact mechanics problem and the determination of the most meaningful modulus.

From the measured values of S, P_{max} and δ_{max}, Equations 8 and 9 are combined to determine A, which represents the contact area between the nanoindenter tip and the sample surface. Young's

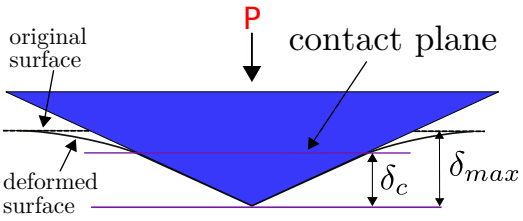

Figure 3: Schematic of an indentation experiment, illustrating the relationship between δ_c and δ_{max}.

modulus can be calculated from the values obtained above through the use of a reduced modulus. The reduced modulus is obtained from the following expression for the contact stiffness, assuming the contact stiffness for a Berkovich tip is the same for a circular contact of the same area:

$$S = \frac{2}{\sqrt{\pi}} E_r \sqrt{A} \tag{10}$$

Here E_r accounts for the contributions from both the indenter and the sample, and is given as follows:

$$\frac{1}{E_r} = \frac{\left(1-\nu^2\right)}{E} + \frac{\left(1-\nu_i^2\right)}{E_i} \tag{11}$$

where E and ν are Young's modulus and Poisson's ratio for the paint coating, respectively, and E_i and ν_i are Young's modulus and Poisson's ratio for the indenter. In our case the indenter is much stiffer than the paint coating ($E_i \gg E$), so Equation 11 is approximated by:

$$E_r \approx \frac{E}{1-\nu^2} \tag{12}$$

Films for nanoindentation were made by hand grinding zinc oxide pigment with alkyd resin with a few drops of solvent and spreading the resulting mixture on glass slides. Samples were cast to a dry thickness of $\sim$ 250µm and aged naturally and artificially. Naturally aged samples were allowed to cure at room temperature for 10 months; mechanical data were collected monthly. One set of samples was naturally aged for 6 months, and then thermally aged at 60 °C in an oven for 100 hours. Another set of samples naturally aged for 5.7 months was exposed to filtered xenon light using a Nikon LH-M100C-1 High Pressure XBO lamp for 172 hours (LH-M100Melville, NY). Ultraviolet and infrared wavelengths were filtered from the light during sample illumination, with total illumination power at the surface of 0.03W over an illuminated area of 8mm$\times$5mm. Films were removed from the oven and light source to collect mechanical data after 5, 10, 25, 50, 75, and 100 hours of artificial aging; these data were collected at room temperature. Nanoindentation data were collected using a Hysitron TI 950 TriboIndenter (St. Eden Prairie, MN) outfitted with a diamond Berkovich tip, the tip radius of which is about 150nm. Continuous load-displacement measurements were recorded during indentation. The indenter penetrated the surface at a constant displacement rate until a predetermined displacement depth of 1200 nm was achieved. After a 5-second hold period, the load was removed from the sample at a constant rate. The reduced elastic modulus, E_r, and hardness values, H, were calculated from the average of up to six indents, each separated by 100µm, using the calculations described below for measurements in the context of viscoelastic materials.

3. Results and Discussion

3.1. Thermogravimetric Determination of Pigment Volume Concentration

Samples were made by adding zinc oxide pigment particles to commercial alkyd formulation at overall weight fractions of 0, 0.2, 0.4 and 0.6. These are the 'wet' weight fractions, w_{ZnO}^{wet}, listed in Table 1. Measurements of the initial weight loss of the unfilled alkyd indicated that 43 wt% of the formulation consisted of volatile solvent that was not present in the dried film. Accounting for this mass loss gives the 'dry' weight fractions, w_{ZnO}^{dry}, as follows:

$$w_{\mathrm{ZnO}}^{dry} = \frac{w_{\mathrm{ZnO}}^{wet}}{w_{\mathrm{ZnO}}^{wet} + 0.57\left(1 - w_{\mathrm{ZnO}}^{wet}\right)} = \frac{w_{\mathrm{ZnO}}^{wet}}{0.43 w_{\mathrm{ZnO}}^{wet} + 0.57} \tag{13}$$

These weight fractions were then converted to volume fractions, φ_{ZnO} by assuming a density of $1.2\mathrm{g/cm}^3$ for the alkyd resin and a density of $5.6\mathrm{g/cm}^3$ [28] for the zinc oxide. This value for the density of the unfilled resin was obtained from the measurements of the thickness, area, and mass of an unpigmented DMA sample. The overall ZnO volume fraction is obtained from the following expression:

$$\varphi_{\mathrm{ZnO}} = \frac{w_{\mathrm{ZnO}}^{dry}/5.6}{\left(w_{\mathrm{ZnO}}^{dry}/5.6\right) + \left(1 - w_{\mathrm{ZnO})}^{dry}\right)/1.2} \tag{14}$$

The density of the dry systems, ρ_{dry} is then given as follows:

$$\rho_{dry}\left(\mathrm{g/cm}^3\right) = 5.6\phi_{\mathrm{ZnO}} + 1.2\left(1 - \phi_{\mathrm{ZnO}}\right) \tag{15}$$

Wet Weight Fraction ZnO (w_{ZnO}^{wet})	Dry Weight Fraction ZnO (w_{ZnO}^{dry})	Dry Volume Fraction ZnO (φ_{ZnO})	Dry Density (ρ_{dry}) g/cm^3	$(d\rho)_{max}$ (from QCM) μm·g/cm^3
0	0	0	1.2	4.3
0.05	0.085	0.019	1.29	4.9
0.10	0.16	0.040	1.38	5.9
0.20	0.30	0.086	1.58	5.9
0.40	0.54	0.20	2.08	8.2
0.50	0.64	0.27	2.40	4.0
0.60	0.72	0.36	2.79	-

Table 1: Pigment composition of Galkyd model system. Density estimates were used to convert weight percentages to volume percentages. Values of $(d\rho)_{max}$ correspond to values obtained from the QCM experiments on the thin-film samples.

Thermogravimetric (TGA) experiments were conducted on naturally aged 5-month-old alkyd samples for four of the zinc oxide filler loadings listed in Table 1 to confirm the amount of zinc oxide pigment present relative to the binder after solvent evaporation. These results are shown in Figure

4. The primary degradation steps of the alkyd resin are observed from 250–480°C [2, 29]. These mass decreases are attributed to oxidative degradation of the alkyd and alkyd combustion [2, 30]. A large mass loss with a steep slope that corresponds to the primary degradation was observed in the 0 vol% ZnO sample (the solid curve in Figure 4), and subsequently in each sample of increasing zinc oxide concentration. The pure alkyd resin did not completely volatilize during the TGA experiment, but left a residue that corresponds to approximately 9% of the dry sample's total weight. The mass remaining at 500 °C, which we refer to as $w(500)$ is consistent with the presence of all of the zinc oxide in addition to 9% of the alkyd resin, as calculated from the following expression:

$$w(500) = w_{\mathrm{ZnO}}^{dry} + 0.09\left(1 - w_{\mathrm{ZnO}}^{dry}\right) \tag{16}$$

These values for $w(500)$ are included as the crosses in Figure 4. These are a consistency check on our result that 43 wt% of the wet alkyd resin is a volatile fraction that evaporates soon after the films are formed, and that 9% of the remaining fraction of the dried alkyd consists of components that do not volatilize until much higher temperatures. For the rest of this paper, the samples will be indicated using the ZnO volume fraction, which ranges from 0 to 0.37.

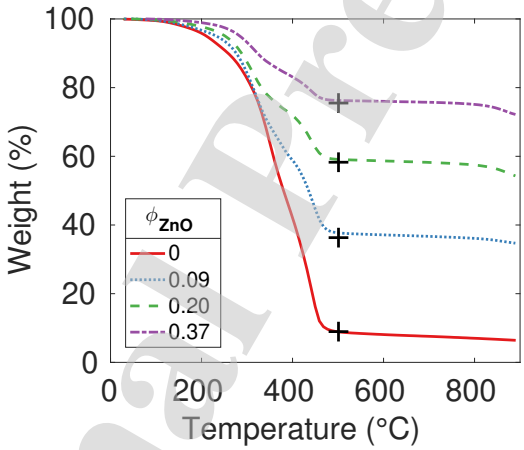

Figure 4: TGA results for the model alkyd system with wet weight percents from 0 to 60 wt% zinc oxide. The crosses correspond to the values obtained from Equation 16.

3.2. Dynamic Mechanical Characterization

Figure 5 shows the results of DMA measurements on pigmented alkyd films, naturally aged for two months. The DMA curves were shifted to a reference temperature of 20 °C by applying a temperature-dependent shift factor a_T in order to show the response over a wide range of frequencies. These shift factors are plotted in Figure 5c. Figure 5a shows $|E^*|$, the magnitude of the complex Young's modulus measured by DMA, as a function of $a_T f$. The unpigmented sample begins at low frequencies in the rubbery regime, going through the glass transition to the glassy regime at higher frequencies, as indicated by the decrease in the phase angle and plateauing of the modulus. The unpigmented sample has a modulus of about 10^9Pa in the glassy regime. The pigmented samples have higher moduli than the unpigmented sample at the same frequencies and

at the lowest frequency they are already leaving the rubbery regime. In Figure 5b, the phase angles are shown as a function of $a_T f$. Each sample shows a peak in the phase angle, corresponding to the glass transition, which occurs at lower frequencies for higher pigment concentrations. The frequency at which the peak occurs decreases from $7 \cdot 10^{-2}$Hz to $6 \cdot 10^{-4}$Hz. This shift in peak indicates that the T_g increases with pigment content. As the pigment concentration increases, the height of the peak decreases from 55° for the unpigmented film to 30° for the 9 vol% film, indicating that the relaxation time distribution broadens as filler is added to the sample. The T_g shift and broadening of the relaxation time distribution are both consistent with a slowing down of the polymer dynamics in the vicinity of the filler particles, an effect that is well documented in nanocomposite systems [31].

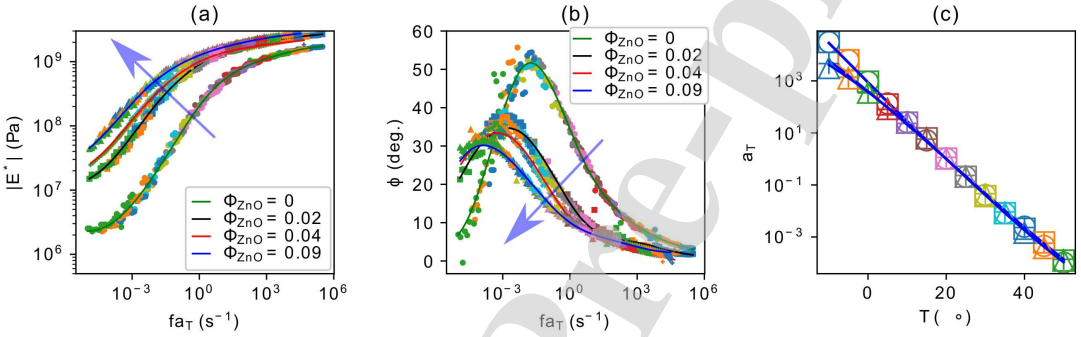

Figure 5: Time-temperature superposition results for alkyd films containing 0%, 2%, 4%, and 9% zinc oxide by volume, after curing at ambient conditions for two months. (a) and (b) show the absolute value of the Young's modulus and the phase angle, respectively, as a function of the measurement frequency multiplied by the shift factor a_T. (c) shows the values of the shift factor a_T as a function of temperature. The arrow in (a) and (b) shows the progression of the curves according to increasing ϕ_{ZnO}. The data are color coded according to temperature, with the colors in (a) and (b) corresponding to the temperatures with the same color in (c).

3.3. High-Frequency Mechanical Characterization (Quartz Crystal Rheometry)

The first piece of information that is obtained from the QCM experiments is the change in total sample mass, which is plotted for the different samples in Figure 6. The mass initially increases as oxygen is incorporated into the film during the initial, oxidative curing steps of the material. This occurs over the first day of cure, with the measured mass increase correlating with the decrease in aliphatic double bonds as quantified by Raman spectroscopy[32]. The mass eventually begins to decrease as volatile compounds are formed and released from the coating. These effects have been discussed in some detail in our previous work with the base, unfilled alkyd[32]. The important and novel aspect point from the point of view of our current work is that the time required to reach the maximum mass is a quantitative measure of the kinetics of the oxidation reactions taking place during the early stages of the curing process. These kinetics are measurably increased by the presence of ZnO, as indicated by the details of the mass changes in the vicinity of the mass maximum, shown in Figure 6b. The time at which the mass is maximized decreases monotonically

with added ZnO, decreasing from ∼20 hrs. for $\phi_{ZnO} = 0$ to ∼10 hrs for $\phi_{ZnO} = 0.27$, indicating a doubling of the rate of oxidation over this range of ZnO concentrations.

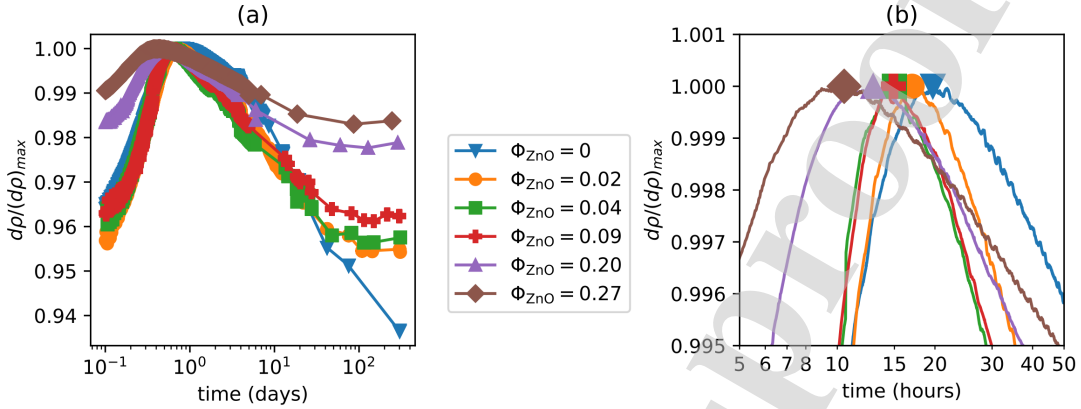

Figure 6: Normalized film mass as a function of curing time for the samples with different filler fractions: a) The entire curve over the range of measured times; b) detail of the data near the maximum in the mass, illustrating the enhanced curing rate as the zinc oxide fraction increases. The symbols in part (b) indicate the maximum on the mass curve, which occurs for shorter times as ϕ_{ZnO} increases. Values of $(d\rho)_{max}$ for each sample are listed in Table 1.

The ability of the QCM to quantify the oxidation kinetics in the alkyd system originates from two features of the this technique. The first is the thin film nature of the technique, which ensures that oxygen diffuses throughout the entire film on time-scales that are much shorter than the time-scale of the measurement. In practical terms, 'skin' effects are avoided because the entire sample can be viewed as the skin layer that would be obtained from a measurement performed on a much thicker sample. The second aspect of the QCM technique is its extraordinary sensitivity to very small mass changes, able to accurately measure mass changes of 1 part in 10,000, as illustrated by Figure 6b. Note that relative mass changes can still be reliably measured, even when a more approximate analysis based on the Sauerbrey equation (Eq. 3) is used to extract the data. Consider, for example, a sample with $d\rho = 5\mu\text{m}\cdot\text{g/cm}^3$, $\left|G_3^*\right|\rho = 10^9\,\text{Pa}\cdot\text{g/cm}^3$, and $\phi = 90°$, values that are typical of the films studied here. The frequency decrease for the third harmonic as obtained from Eq. 4 for this set of parameters is 91,598 Hz, 8 % larger than the Sauerbrey prediction of Eq. 84,841 Hz obtained from Eq. 3. Straightforward application of the Sauerbrey equation to interpret the mass data in the vicinity of the mass maximum will simply shift the mass curve downward by 8%, which when normalized by the maximum value will give curves virtually identical to those shown in Figure 6.

Deviations from the Sauerbrey equation are still important, however, in that they enable the mechanical properties to be accurately quantified. This ability emerges from the additional information obtained from the dissipation (Γ in our notation) and the ability to quantify the difference between the measured value of the frequency shift and the Sauerbrey prediction. These differences are only meaningful when data from two harmonics, typically $n = 3$ and $n = 5$ are obtained. This is because the mass itself is unknown initially, so deviations from the Sauerbrey scaling are

quantified as deviations from the linear scaling between n and Δf_n that is predicted by Eq. 3. In Figure 7 we show the properties obtained by forcing the measured values of Δf_3, Δf_5 and $\Delta\Gamma_3$ to the values predicted from Eq. 4. We refer to this calculation as a 3:5,3 calculation, and it is the most reliable calculation for this particular set of material properties. A 1:3,3 calculation was used to generate the data in Figure 6 because because the resonance peak for $n = 5$ cannot be reliably obtained during the early stages of cure in these materials.

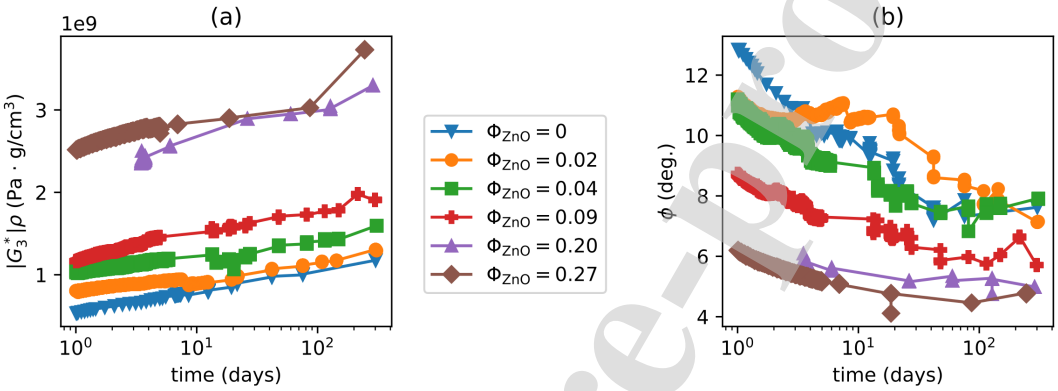

Figure 7: High frequency rheometric data for an alkyd resin filled with zinc oxide: a) product of the film density and the magnitude of the complex shear modulus of the film at 15 MHz (b) phase angle of the complex shear modulus at 15 MHz.

The data in Figure 7 indicate that the time evolution of the mechanical properties during the later stages of cure are qualitatively similar, with the magnitude of the complex shear modulus showing a similar increase over time for all filler loadings. The effect of the filler is to stiffen the system in a way that is largely consistent with Eq. 1, as illustrated in Figure 8. Here we plot relationship between $\left|G_3^*\right|$ and ϕ_{ZnO} at a cure time of 20 days, using the data from Figure 7a and the densities listed in Table 1. The data are described by Eq. 1, using $\left|G_3^*\right|$ for G and with G_0= 7.1x10^8 Pa and ϕ^*=0.64. This is by no means a unique functional form, but is given as point of comparison to a commonly used filler model. Deviations are observed at the highest ZnO concentrations, which we attribute to the non-ideal nature of the particles and the difficulty in getting a macroscopically uniform sample for the quantitative QCM experiment for this particular sample.

3.4. Nanoindentation

While the QCM and DMA techniques are very well suited for investigations of well-controlled model films with defined geometries, these techniques are generally ill-suited for investigations of historic paint films due to the size-limited nature of samples that can be taken from works of art. Nanoindentation can be performed on very small samples, and is a technique that is well-positioned to impact the field of conservation science[33]. SEM images of some of the ZnO-filled systems investigated here are shown in Figure9. Figure 9a depicts the small zinc oxide particles (in white) scattered throughout the alkyd matrix (in gray); there are portions of pigment-poor matrix clearly visible. The paint film appears to be more homogeneously filled in the 20 vol% zinc oxide sample

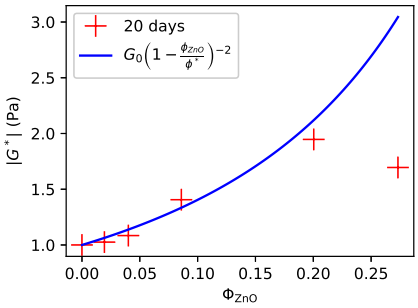

Figure 8: Shear moduli determined from the QCM experiments at a cure time of 20 days. The solid line corresponds to Eq. 1, with G_0= 7.1x10^8 Pa and ϕ^*=0.64.

(Figure9b). In the 37 vol% zinc oxide film, the matrix is very densely packed with an even more homogeneous distribution of pigment particles (Figure9c). As a point of comparison, the critical pigment volume concentration for a zinc-oxide commercial paint is is $\sim$ 50% or less. Previous work on Ripolin, an early oil-based paint used by many avant-garde artists including Pablo Picasso (1881-1973) was shown to have a similarly homogeneously packed distribution of ZnO pigment particles. Furthermore, thermogravimetric analysis of Ripolin paints gave values of 63.5 wt% solid residue (assumed to be mostly pigment) and 36.5% binder [34].

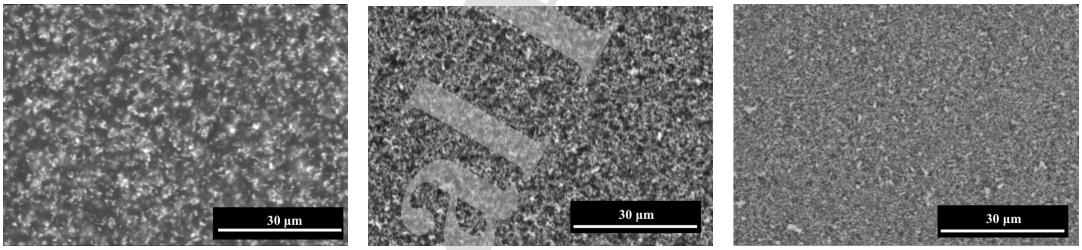

(a) 9 vol% **(b)** 20 vol% **(c)** 37 vol%

Figure 9: Pigment particle packing at different volume fractions in samples for nanoindentation: 9% (a), 20% (b), and 37% (c). As the pigment content increases, pigment particles pack more closely and begin to aggregate.

The reduced modulus and hardness of naturally and artificially aged pigmented films were measured over time. As with DMA, films could not be measured as soon as they were made because the films were insufficiently stiff, so the first measurements were made after one month of curing. Figure10 shows the mechanical properties of alkyd resins with different pigment concentrations plotted as a function of time. Figure 10a shows the results of natural aging, at room temperature and ambient humidity. These plots show that the reduced modulus and hardness increase with pigment concentration and with time. While all films show increasing modulus and hardness with time and pigment content, the largest increase is observed in the 9 vol% sample between 0 and 150 days. Both modulus and hardness increase by approximately one order of magnitude, suggesting that the 9 vol% films behave as if they have a higher filler content.

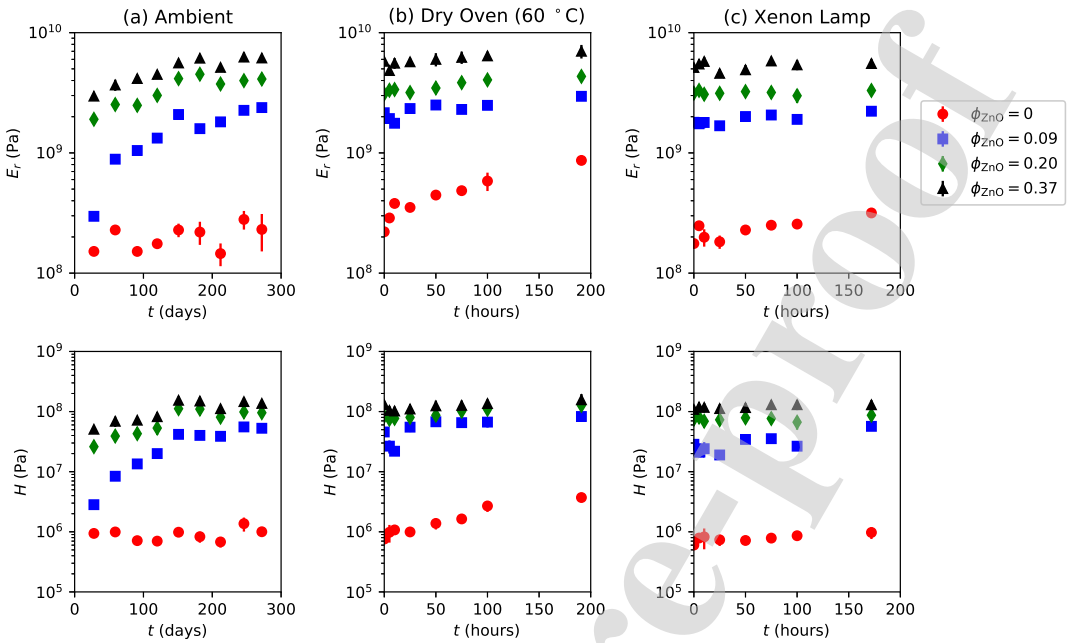

Figure 10: Mechanical properties of alkyd model systems over time. (a) reduced modulus and hardness of paint films with increasing pigment content aged for 10 months; (b) reduced modulus and hardness of paint films aged up to 100 hours in a dry oven after 6 months of curing at room temperature; (c) reduced modulus and hardness of films aged up to 172 hours with a xenon lamp after 5.7 months of curing at room temperature.

Figure 10b shows the effects of aging in a 60°C oven after 6 months of natural aging. The trend is towards increased modulus and hardness with exposure to higher temperatures, but there is significant scatter in the data and longer times need to be investigated to verify and quantify the effect. Figure10c shows the effects of aging with a xenon lamp on pigmented films after 5.7 months of natural aging. After 172 hours of light exposure there is no significant change in the modulus, and the hardness only increases for the 9 vol% sample. At these time scales there are no significant differences between the aging effects of the different pigment concentrations.

Regardless of the age of the paint film or the mode of artificial aging to which it was subjected, the normalized modulus and hardness values increase with increasing zinc oxide content, with very little change in the modulus of the unfilled polymer, for which $G \approx 10^9$ Pa in nearly all cases. In a measurement of a historic paint sample, the local properties will be most strongly affected by the inorganic content, which is generally not known. Fortunately, other properties can be extracted from an indentation experiment, including the creep or stress relaxation behavior [33], and these experiments are likely to play a role in the future. Also, looking at the effects of the temperature on an aged sample, or the effect of very high humidity or solvent vapor on the mechanical properties of the film can also provide information. These approaches have been utilized in our QCM work[26, 32, 35], and a similar philosophy is likely to be valuable for future nanoindentation experiments as well.

3.5. Technique Comparison

Each of the three techniques employed here provides a different type of information about the mechanical properties of ZnO-pigmented alkyd resins. DMA measurements span the widest range of frequencies, with nanoindentation probing only the low-frequency response and quartz crystal rheometry probing only the high-frequency response. All of these techniques show an increase in the elastic stiffness of the material with increasing pigment concentration. To compare the values measured by each of these techniques in a quantitative way, however, some conversions have to be made. DMA measures E^*, nanoindentation E_r, and quartz crystal rheometry $|G^*|\rho$ and ϕ. Since no phase angle information was obtained from the nanoindentation data, the comparison must consist of the magnitude of the modulus only. The reduced modulus, E_r, can be converted to a value of E^* by assuming $E_r = |E^*| / \left(1-\nu^2\right)$ consistent with Equation 12. Poisson's ratio is generally close to 0.5 for the situations of interest to us. A lower bound for Poisson's ratio is obtained by assuming a value of $K \approx 3.5 10^9$ Pa for the bulk compressive modulus, close to the value obtained for both neat polystyrene and polystyrene with 10 wt.% silica filler [36]. We then obtain ν from the following expression, with this fixed value of K:

$$\nu = \frac{3 - 2\,|G^*|\,/K}{6 + 2\,|G^*|\,/K} \tag{17}$$

In the rubbery regime G/K is small enough so that ν for our purposes is indistinguishable from 0.5. In the glassy regime, $G/K \approx 0.3$, which gives $\nu \approx 0.36$.

Similarly, the following equation can be used to convert $|G^*|$ to $|E^*|$:

$$|E^*| = 2|G^*|(1+\nu) \tag{18}$$

When comparing the quartz crystal rheometry and nanoindentation results, it is important to account for the orders of magnitude difference in the frequency at which these measurements were taken. Fortunately, the dynamic mechanical measurements provide a bridge between these two techniques. This point is illustrated by the data in Figure 11, where we plot the frequency dependence of $|E^*|$ for data obtained by nanoindentation, quartz crystal rheometry and DMA, referenced to room temperature. The nanoindentation measurements were not taken cyclically, but based on the indentation rate they are plotted here at a frequency of 1Hz, since the timescale of the unloading portion of the experiment from which the modulus is determined is about 1 second. When the relevant time scales of the different experiments are accounted for appropriately, we see that the moduli measured by the different techniques are in good agreement with one another.

A convenient way to plot dynamic mechanical data without accounting for frequency-dependent or time-dependent shift factors is to plot the phase angle as a function of the magnitude of the modulus. These plots, closely related to van Gurp-Palmen plots that have been used previously as a test of the validity of time-temperature superposition[37, 38], give a useful representation of dynamic mechanical data. The DMA and QCM data from our experiments are plotted in this form in Figure 11b. For a given sample, one moves from left to right on the van Gurp-Palmen plot either by decreasing the temperature or increasing the frequency. The maximum in the phase angle is proportional to the maximum in the slope of $\log(|E^*|)$ vs. $\log(fa_T)$,[26]. This slope is

in turn related to the distribution of relaxation times in the material, with a lower slope indicative of a broader relaxation time distribution. Two additional aspects of Figure 11b are noteworthy. First, the van Gurp-Palmen curves from the DMA measurements at frequencies from 0.1 to 10 Hz overlap with one another in the glassy regime, indicating that these glassy systems share some features that are independent of the filler content. Second, the QCM data obtained at a frequency of 15 MHz are shifted to higher moduli by a factor of about 2 in comparison to the DMA data, reminiscent of the behavior observed in filled silicone systems consisting of nanoscale regions with different dynamic properties [39]. These results are an excellent starting point for further detailed investigations of the mechanics of these systems, ideally including model systems that are more fully understood than the commercial alkyd system used in our experiments.

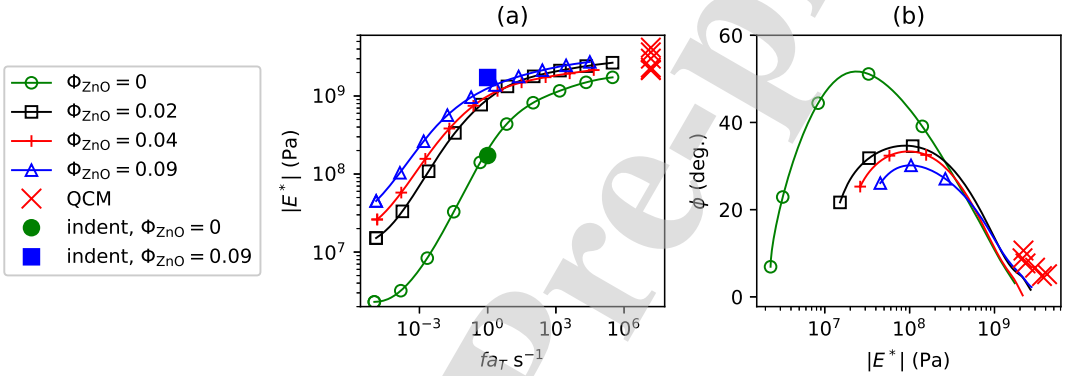

Figure 11: a) DMA data from Figure 5a, plotted along with the moduli extracted from the quartz crystal rheometry measurements at a frequency of 15 MHz, and the nanoindentation data, where we assume an effective frequency of ≈1 Hz. b) DMA and QCM data plotted in the van Gurp-Palmen form. All data were obtained from samples that had been cured for two months.

4. Conclusions

We have used three different mechanical experiments (DMA, QCM, and nanoindentation) to probe the mechanical response over time of a commercial alkyd system filled with different concentrations of ZnO. Dynamic mechanical analysis can probe a wide range of frequencies, but the measurements require a large amount of sample and are only possible once the material forms a free-standing film. The quartz crystal rheometer gives viscoelastic measurements at a single frequency and additionally provides mass data and is able to measure changes in time from the onset of the cure process. It also uses very thin films, avoiding skin effects that plague thicker samples needed for the DMA experiments. These thin films, however, can be very difficult to obtain for the high filler loadings that are typical of many commercially viable paints. Nanoindentation probes the Young's modulus and hardness at low frequencies, and these measurements are the ones most comparable to hardness measurements common in the paint community. Films must be already partially cured before nanoindentation can be performed, but a number of measurements can be taken simultaneously and the sample required is small. Quartz crystal rheometry

measures at very high frequencies (15 MHz), and gives results in good agreement with the DMA and nanoindentation when the timescale of each measurement is taken into account. The following materials-related conclusions emerged from this work.

- The elastic modulus of the samples increases with ZnO concentration and with curing time in ways that can be described by existing models of the elastic properties of filled polymers.
- The ZnO filled samples have a higher glass transition temperature and broader relaxation time distribution than the unfilled samples, a result that is consistent with a slowing of the polymer dynamics in the immediate vicinity of a ZnO surface.
- Oxidation of the polymer during the early stages of cure as measured by the QCM occurs more quickly with increasing ZnO filler fractions. At the highest filler fractions this process happens about twice as fast when compared with the unfilled system.

The last of these results is particularly noteworthy in that it shows that the quartz crystal rheometer can be a particularly valuable tool for assessing the long-term aging of paint coatings. Effects that can be investigated include the effect of environmental conditions and of specific additives on cure behavior at all stages of the curing process, provided that samples with a thickness of $\sim 5\,\mu$m and a macroscopic lateral homogeneity over $\sim$ 1cm can be produced. These experiments complement nanoindentation measurements in paint films at high particle concentration (such as in historic paint films) which can be performed on small samples of historic paint samples but are affected by the filler fraction and details of the filler particle dispersion.

5. Acknowledgments

This material is based upon work supported by the National Science Foundation through the Division of Materials Research (DMR-1241667), the Office of International Science and Engineering (OISE-1743748) and the Graduate Research Fellowship program (DGE-1324585). The Andrew W. Mellon Foundation and the Grainger Foundation are thanked for their support of scientific research at the Art Institute of Chicago. This work made use of the EPIC and SPID facilities of the NUANCE Center at Northwestern University, which has received support from the Soft and Hybrid Nanotechnology Experimental (SHyNE) Resource (NSF NNCI-1542205); the MRSEC program (NSF DMR-1121262) at the Materials Research Center; the International Institute for Nanotechnology (IIN); the Keck Foundation; and the State of Illinois, through the IIN.

6. References

[1] M. F. Mecklenburg, C. S. Tumosa, E. P. Vicenzi, The Influence of Pigments and Ion Migration on the Durability of Drying Oil and Alkyd Paints, Smithsonian Contributions to Museum Conservation (2013) 59–6700000.

[2] C. Duce, L. Bernazzani, E. Bramanti, A. Spepi, M. P. Colombini, M. R. Tiné, Alkyd artists' paints: Do pigments affect the stability of the resin? A TG and DSC study on fast-drying oil colours, Polymer Degradation and Stability 105 (2014) 48–58. doi:10.1016/j.polymdegradstab.2014.03.035.

[3] W. K. Asbeck, M. V. Loo, Critical Pigment Volume Relationships., Ind. Eng. Chem. 41 (7) (1949) 1470–1475. doi:10.1021/ie50475a042.

[4] A. Toussaint, Influence of pigmentation on the mechanical properties of paint films, Progress in Organic Coatings 2 (3) (1974) 237–267. doi:10.1016/0300-9440(74)80004-4.

[5] D. Y. Perera, Effect of pigmentation on organic coating characteristics, Progress in Organic Coatings 50 (4) (2004) 247–262. doi:10.1016/j.porgcoat.2004.03.002.

[6] E. Hagan, M. Charalambides, T. J. Learner, A. Murray, C. Young, Factors affecting the mechanical properties of modern paints, in: Modern Paints Uncovered: Proceedings from the Modern Paints Uncovered Symposium, 2007, pp. 225–233.

[7] I. M. Krieger, T. J. Dougherty, A Mechanism for Non-Newtonian Flow in Suspensions of Rigid Spheres, Transactions of the Society of Rheology 3 (1) (1959) 137–152. doi:10.1122/1.548848.

[8] I. M. Krieger, Rheology of monodisperse latices, Advances in Colloid and Interface science 3 (2) (1972) 111–136.

[9] T. Shikata, D. S. Pearson, Viscoelastic behavior of concentrated spherical suspensions, Journal of Rheology 38 (3) (1994) 601–616. doi:10.1122/1.550477.

[10] J. Bicerano, J. F. Douglas, D. A. Brune, Model for the Viscosity of Particle Dispersions, Journal of Macromolecular Science, Part C 39 (4) (1999) 561–642. doi:10.1081/MC-100101428.

[11] J. W. Bullard, A. T. Pauli, E. J. Garboczi, N. S. Martys, A comparison of viscosity–concentration relationships for emulsions, Journal of Colloid and Interface Science 330 (1) (2009) 186–193. doi:10.1016/j.jcis.2008.10.046.

[12] J. Mewis, N. Wagner, Colloidal Suspension Rheology, Cambridge University Press, 2012.

[13] G. Osmond, J. J. Boon, L. Puskar, J. Drennan, Metal Stearate Distributions in Modern Artists' Oil Paints: Surface and Cross-Sectional Investigation of Reference Paint Films Using Conventional and Synchrotron Infrared Microspectroscopy, Appl. Spectrosc. 66 (10) (2012) 1136–1144.

[14] G. Osmond, Zinc white: A review of zinc oxide pigment properties and implications for stability in oil-based paintings, AICCM Bulletin 33 (1) (2012) 20–29, 00015. doi:10.1179/bac.2012.33.1.004.

[15] J. J. Hermans, K. Keune, A. van Loon, R. W. Corkery, P. D. Iedema, The molecular structure of three types of long-chain zinc(II) alkanoates for the study of oil paint degradation, Polyhedron 81 (2014) 335–340, 00009. doi:10.1016/j.poly.2014.06.030.

[16] J. J. Hermans, K. Keune, A. van Loon, P. D. Iedema, An infrared spectroscopic study of the nature of zinc carboxylates in oil paintings, J. Anal. At. Spectrom. 30 (7) (2015) 1600–1608, 00010. doi:10.1039/C5JA00120J.

[17] F. Gabrieli, F. Rosi, A. Vichi, L. Cartechini, L. Pensabene Buemi, S. G. Kazarian, C. Miliani, Revealing the Nature and Distribution of Metal Carboxylates in Jackson Pollock's Alchemy (1947) by Micro-Attenuated Total Reflection FT-IR Spectroscopic Imaging, Anal. Chem. 89 (2) (2017) 1283–1289. doi:10.1021/acs.analchem.6b04065.

[18] F. Casadio, K. Keune, P. Noble, A. van Loon, E. Hendriks, S. Centeno, Metal Soaps in Art: Conservation and Research, Cultural Heritage Science, Springer International Publishing, 2019.

[19] H. Kühn, Zinc White, in: R. L. Feller (Ed.), Artists' Pigments: Volume 1: A Handbook of Their History and Characteristics, Cambridge University Press, Washington, 1987, 00047.

[20] M. Mecklenburg, C. Tumosa, D. Erhardt, The changing mechanical properties of aging oil paints, Materials Issues in Art and Archaeology VII 852 (2005) 13–24.

[21] D. Johannsmann, Viscoelastic analysis of organic thin films on quartz resonators, Macromol. Chem. Phys. 200 (1999) 501–516.

[22] G. Sauerbrey, Verwendung von Schwingquarzen zur Wägung dünner Schichten und zur Mikrowägung, Zeitschrift für Physik A Hadrons and Nuclei 155 (2) (1959) 206–222. doi:10.1007/BF01337937.

[23] D. Johannsmann, Viscoelastic, mechanical, and dielectric measurements on complex samples with the quartz crystal microbalance, Phys. Chem. Chem. Phys. 10 (31) (2008) 4516–4534.

[24] D. A. Brass, K. R. Shull, Membrane-enhanced surface acoustic wave analysis of grafted polymer brushes, Journal of Applied Physics 103 (7) (2008) 073517. doi:10.1063/1.2903880.

[25] G. C. DeNolf, L. F. Sturdy, K. R. Shull, High-Frequency Rheological Characterization of Homogeneous Polymer Films with the Quartz Crystal Microbalance, Langmuir 30 (32) (2014) 9731–9740. doi:10.1021/la502090a.

[26] D. E. Delgado, L. F. Sturdy, C. W. Burkhart, K. R. Shull, Validation of quartz crystal rheometry in the megahertz frequency regime, Journal of Polymer Science Part B: Polymer Physics 10.1002/polb.24812. doi:10.1002/polb.24812.

[27] W. C. Oliver, G. M. Pharr, An Improved Technique For Determining Hardness and Elastic-Modulus Using Load and Displacement Sensing Indentation Experiments, J. Mater. Res. 7 (6) (1992) 1564–1583. doi:10.1557/JMR.1992.1564.

[28] H. G. Völz, J. Kischkewitz, P. Woditsch, A. Westerhaus, W.-D. Griebler, M. De Liedekerke, G. Buxbaum, H. Printzen, M. Mansmann, D. Räde, G. Trenczek, V. Wilhelm, S. Schwarz, H. Wienand, J. Adel, G. Adrian, K. Brandt, W. B. Cork, H. Winkeler, W. Mayer, K. Schneider, L. Leitner, H. Kathrein, E. Schwab, H. Jakusch, M. Ohlinger, R. Veitch, G. Etzrodt, G. Pfaff, K.-D. Franz, R. Emmert, K. Nitta, R. Besold, H. Gaedcke, Pigments, Inorganic, in: Ullmann's Encyclopedia of Industrial Chemistry, Wiley-VCH Verlag GmbH & Co. KGaA, 2000, 00015.

[29] M. Lazzari, O. Chiantore, Drying and oxidative degradation of linseed oil, Polymer Degradation and Stability 65 (2) (1999) 303–313. doi:10.1016/S0141-3910(99)00020-8.

[30] R. Ploeger, D. Scalarone, O. Chiantore, Thermal analytical study of the oxidative stability of artists' alkyd paints, Polymer Degradation and Stability 94 (11) (2009) 2036–2041. doi:doi:10.1016/j.polymdegradstab.2009.07.018.

[31] H. Lu, S. Nutt, Restricted Relaxation in Polymer Nanocomposites near the Glass Transition, Macromolecules 36 (11) (2003) 4010–4016, 00206. doi:10.1021/ma034049b.

[32] L. F. Sturdy, A. Yee, F. Casadio, K. R. Shull, Quantitative characterization of alkyd cure kinetics with the quartz crystal microbalance, Polymer 103 (2016) 387–396. doi:10.1016/j.polymer.2016.09.063.

[33] J. Salvant, E. Barthel, M. Menu, Nanoindentation and the micromechanics of Van Gogh oil paints, Applied Physics A 104 (2011) 509–515. doi:10.1007/s00339-011-6486-x.

[34] K. Muir, G. Gautier, F. Casadio, A. Vila, Interdisciplinary investigation of early house paints: Picasso, Picabia and their "Ripolin" paintings., in: J. Bridgeland (Ed.), ICOM Committee for Conservation Preprints, Critério - Artes Gráficas, Lda, Lisbon, 2011.

[35] L. Sturdy, F. Casadio, M. Kokkori, K. Muir, K. R. Shull, Quartz crystal rheometry: A quantitative technique for studying curing and aging in artists' paints, Polymer Degradation and Stability 107 (2014) 348–355. doi:10.1016/j.polymdegradstab.2014.02.009.

[36] R. Tao, S. L. Simon, Bulk and shear rheology of silica/polystyrene nanocomposite: Reinforcement and dynamics, Journal of Polymer Science Part B: Polymer Physics 53 (9) (2015) 621–632. doi:10.1002/polb.23669.

[37] van Gurp, J. Palmen, Time-Temperature Superposition for Polymeric Blends, Rheol. Bull. 67 (1998) 5–8.

[38] S. Trinkle, C. Friedrich, Van Gurp-Palmen-plot: A way to characterize polydispersity of linear polymers, Rheol. Acta 40 (4) (2001) 322–328. doi:10.1007/s003970000137.

[39] C. J. Yeh, M. Dowland, R. G. Schmidt, K. R. Shull, Fracture and thermal aging of resin-filled silicone elastomers, J. Polym. Sci. Part B: Polym. Phys. 54 (2016) 263–273. doi:10.1002/polb.23919.

-Zinc oxide accelerates the oxidative curing of alkyd paints.
-Consistent results obtained with nanoindentation, dynamic mechanical analysis and high frequency rheometry.

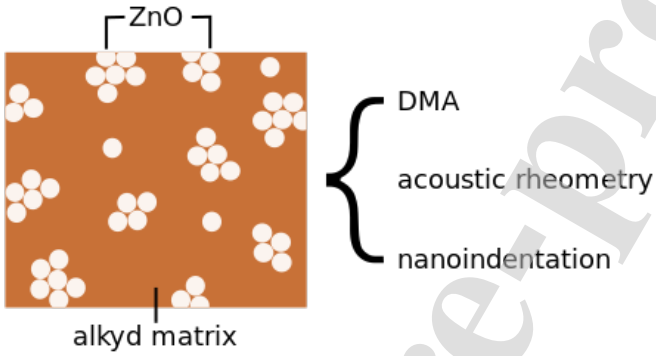

Declaration of interest: none

LF Sturdy: Investigation, Formal Analysis, Writing - Original Draft
MS Wright: Investigation
A Yee: Investigation
F Casadio: Conceptualization, Writing - Reviewing and Editing
KT Faber: Conceptualization, Writing - Reviewing and Editing
KR Shull: Conceptualization, Supervision, Writing - Reviewing and Editing